reactions

MDPI

Article

Elucidation of Possible Reaction Mechanism and Catalyst Design via Kinetic Modeling: Case Studies in Hydrogenation Reactions

Philippe M. Heynderickx [1,2,*] and Dmitry Yu. Murzin [3]

[1] Center for Green Chemistry and Environmental Biotechnology (GREAT), Ghent University Global Campus, 119-5 Songdomunhwa-Ro, Yeonsu-Gu, Incheon 406-840, Republic of Korea
[2] Department of Green Chemistry and Technology, Faculty of Bioscience Engineering, Ghent University, 653 Coupure Links, B-9000 Ghent, Belgium
[3] Johan Gadolin Process Chemistry Centre, Åbo Akademi University, Henriksgatan 2, FI-20500 Turku, Finland; dmurzin@abo.fi
* Correspondence: philippe.heynderickx@ghent.ac.kr

Abstract

Catalyst materials are typically synthesized with distinct composition, and they are evaluated for their specific reaction in terms of conversion and selectivity. In this respect, it can be anticipated that an intermediate composition often leads to the best catalyst. In order to establish this specific composition, this work presents the practical use of kinetic modeling when typical conversion and selectivity versus reaction time experimental data are provided. Specific examples from catalytic hydrogenation reactions starting from citral, cinnamaldehyde, and dicyclopentadiene are used. In the first two cases, the effect of catalyst composition and the influence of prereduction treatment are linked to kinetic hydrogenation parameters, from which it was clear that, e.g., the prereduction speeds up both desired and unwanted reaction paths. For the latter example, it is shown that extracted kinetic data, together with physical characterizations, such as XPS, and chemical characterization such as H_2-TPR, can serve as a basis for optimization of catalyst design leading to possible superior catalytic activity or selectivity.

Keywords: hydrogenation reaction; practical kinetic modeling; catalyst design

1. Introduction

Kinetic studies provide a powerful tool for a better understanding of catalysis and catalytic performance. They form the basis of more accurate reactor design or to acquire deeper insights in the operation of an existing reactor [1,2]. The descriptive power of kinetic modeling for heterogeneous catalysis applications can vary from simple first-order reactions to complex reaction networks including all possible adsorption, dissociation, surface reaction and desorption steps. It is often encountered that, in the case of complex models, the data treatment and corresponding parameter estimation are tedious and difficult tasks from time to time without any end to complete the job satisfactorily.

Sometimes, heterogeneous catalytic data are described via a first-order pseudo-homogeneous kinetic model. For example, Bertero et al. [3–5] and Busygin et al. [6] describe hydrogenation reactions without taking into account adsorption phenomena, since hydrogenation requires dissociative adsorption of H_2 onto a catalyst surface. In another study, Venkatesan et al. [7] studied the hydrodeoxygenation kinetics of syringol, guaiacol and phenol over H-ZSM-5 and, as H_2 was present at a high concentration, all the reactions were assumed to be pseudo-first-order in the concentration of the phenolic compound.

Academic Editor: Luis M. Gandía

Received: 30 March 2026
Revised: 28 June 2026
Accepted: 7 July 2026
Published: 9 July 2026

Other example reactions of this methodology can be found in the kinetics for sucrose and fructose conversion into hydroxymethylfurfural [8–10], the oxidative dehydrogenation of hydrocarbons [11–13] and the description of hydrodesulfurization reactions [14].

Next to modeling, it can be very useful for catalyst design and interpretation of proposed reaction schemes to put forward the so-called 'structure–activity relations' from experimental data. These are commonly reported in catalysis; for example, Cantrell et al. [15] studied a series of $[Mg_{1-x}Al_x(OH)_2]^{x+}(CO_3)_{x/n}{}^{2-}$ hydrotalcite materials with compositions x = 0.25–0.55 and a clear relation between reaction rate for biodiesel synthesis and catalyst basicity, invoked by the Mg^{2+} ion, was reported. Other examples can be found in the selective oxidation of hydrocarbons, for example, n-butane to maleic anhydride, where systems of supported vanadia catalysts are well-studied via these structure–activity relations [16–18]. Selective redox catalysis via catalyst properties such as ionization potential and optical basicity is well-described in the work of Bordes et al. [19–21], where structural defects and the addition of promoters are addressed. Examples from other reactions are the reduction of water into hydrogen via a series of cobalt(II) complex catalysts [22], alkene hydrogenation on iron–cobalt catalysts [23] or/and supported metal clusters [24] and alkene metathesis reactions [25].

Related to the structure–reactivity relations are the well-known catalyst synergistic effects, originating from the combination of two metals in an oxide matrix as they can produce materials with novel structural or electronic properties that can lead to superior catalytic activity or selectivity [26–28]. Sometimes these synergistic effects are successfully coupled to the corresponding reaction kinetics, which gives more information and mechanistic insight into the given reaction. For example, Wang et al. [29] discuss the use of copper oxide supported on samaria-doped ceria for CO oxidation to illustrate interfacial metal oxide–support interaction and synergism. Examples of total oxidation of carbon monoxide and hydrocarbons on Cu-Ce oxides are reported using Langmuir–Hinshelwood reaction rates with a pronounced link to catalytic properties [30,31]. Other examples can be given for hydrogenation reactions over Co-Mo and Ni-Mo MgO supported catalysts [32] and hydrodesulfurization over Rh/TiO_2 catalysts [33].

In this work, a simple tool to obtain kinetics for chemical reactions is provided without enduring the tedious burden of specific programming. Although the presented procedure is not new, this manuscript offers a rigorous approach via an easily accessible Excel spreadsheet, without having to become an expert in programming and without the need for a special software license. This manuscript gives some explicit examples of kinetic modeling where the results point out that earlier proposed reaction schemes can be reshaped or that, with respect to catalyst design and engineering, further optimization is possible after inspection of the experimental data. In other words, the focus of this work is not on the actual experiment or catalyst synthesis as such, but it provides some examples on how experimentally obtained data can be used to extract kinetic information for further catalyst design or improvement in interpretation of the data.

This work shows that a good combination between the inventory of (1) catalyst physical properties, such as composition (surface or bulk), crystallite structure. . ., (2) catalyst chemical properties, such as experimental conversion and selectivity (product distribution), and (3) corresponding kinetic parameters for elucidation of proposed mechanistic pathways and knowledge of reaction coefficients can serve a higher goal in catalyst design and interpretation of catalytic data.

2. Materials and Methods

Three examples are used as a showcase: (1) citral hydrogenation over Ag^0 and Co^0 nanocolloids [34], (2) hydrogenation of cinnamaldehyde over thermo-responsive polymer

grafted carbon nanotubes [35] and (3) hydrogenation of dicyclopentadiene, using Mo on Ni-based catalysts in the hydrogenation of dicyclopentadiene [36]. The original data and specific references to it can be found in Section S.1 from the Supplementary Materials. Based on the obtained kinetic parameters, the complementary strength of kinetic modeling with regard to data interpretation and future catalyst design is presented. The specific details on catalyst synthesis and experimental design, results, error analysis and uncertainties can be found in references [34–36].

In all the addressed examples, the reactions are performed in an isothermal (autoclave) batch reactor, so that the overall continuity equation (CE) for compound A has the form (1) with V, C_A, R_A and t the reactor volume (L), concentration of compound A (mol L^{-1}), the volumetric production rate of compound A (mol s^{-1} L^{-1}) and the reaction time (s):

$$\frac{d(VC_A)}{dt} = VR_A \quad (1)$$

It can be noted that—in the case that the reaction rates are expressed per mass catalyst—the catalyst bulk density can be inserted. Since the reactor is considered to be operated under isothermal conditions, there is no need for an energy balance. If it is assumed that the reaction volume does not significantly change during the reaction, both V terms cancel out and the CE has the form (2):

$$\frac{dC_A}{dt} = R_A \quad (2)$$

All hydrogenation reactions are performed as such that the total hydrogen pressure is kept constant [34–36] and, as such, the concentration of dissolved H_2 is taken constant during reaction. The corresponding concentration dependency is taken up in the reaction coefficient to give pseudo-homogeneous kinetic models, as exemplified in the Introduction [3,5,6,37].

Lastly, all initial conditions (7), (8), (13), (14), (20) and (21) for the examples in the next sections correspond to the fact that no intermediate or products were initially fed. It can be mentioned that, as a lot of acronyms are used in this work (mentioned at the end of this manuscript), a complete list of symbols and acronyms is added to Section S.2 from the Supplementary Materials.

2.1. Citral Hydrogenation

The selective hydrogenation of α,β-unsaturated aldehydes into the corresponding allylic alcohols has a significant industrial importance, but it brings along quite some challenges from both fundamental and practical points of view due to their complex reaction pathways and resulting various products [35,38,39]. An example is the hydrogenation of citral (C) into the corresponding allyl alcohol (AA), which is the product of interest, and citronellal (CN), which is an undesired product, see Scheme 1. Both reactions are considered to be first-order [34], with respective reaction coefficients k_1 and k_2. Formation of other undesired reaction products is modeled via first-order consecutive reactions for C, CN and AA, with reaction coefficients k_3 to k_5:

$$\frac{dC_C}{dt} = -k_1C_C - k_2C_C - k_3C_C \quad (3)$$

$$\frac{dC_{AA}}{dt} = k_1C_C - k_4C_{AA} \quad (4)$$

$$\frac{dC_{CN}}{dt} = k_2C_C - k_5C_{CN} \quad (5)$$

$$\frac{dC_P}{dt} = k_3C_C + k_4C_{AA} + k_5C_{CN} \quad (6)$$

$$(C_C)_{t=0} = C_{C,0} \quad (7)$$

$$(C_{CN})_{t=0} = (C_{AA})_{t=0} = (C_P)_{t=0} = 0 \quad (8)$$

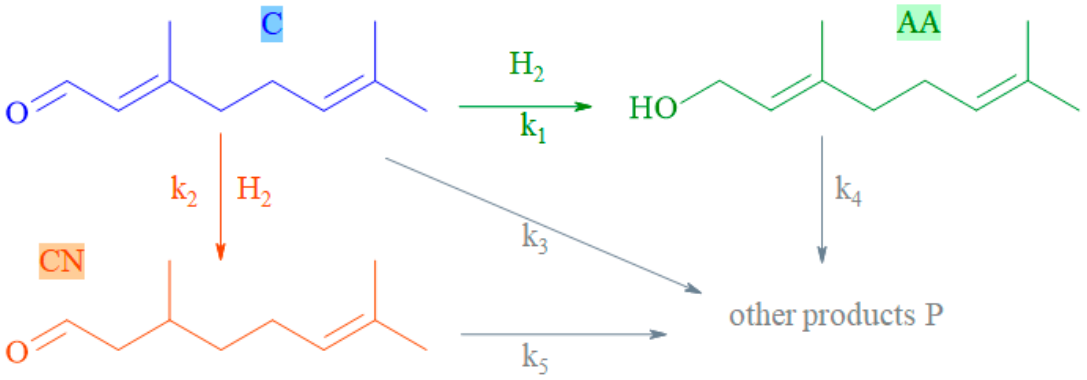

Scheme 1. Hydrogenation of citral ((2E)-3,7-dimethylocta-2,6-dienal or C) into citronellal (3,7-dimethyloct-6-enal or CN), and the allyl alcohol ((2E)-3,7-dimethylocta-2,6-dien-1-ol or AA), which can both react into other products P [34].

Integration of Equations (3)–(6) with initial conditions (7) and (8) gives the time-dependent functions for the corresponding concentration values of C, CN, AA and P, see Section S.3 of the Supplementary Materials for closed form expressions. Relative concentrations are used since the original papers contain conversion and selectivity values, which are always between 0 and 1 mol mol^{-1}. The yield is obtained from reported conversion and selectivity values.

The corresponding Equations (3)–(6) consider concentrations of the compounds (the initial reactant and all products). Considering a constant reaction volume (V), the concentrations are readily convertible into moles ($n = C \cdot V$). Secondly, the product of conversion (X, in $\mathrm{mol_{converted}/mol_{initial}}$) and the selectivity ($S$, in $\mathrm{mol_{product}/mol_{converted}}$) gives the yield ($Y$, in $\mathrm{mol_{product}/mol_{initial}}$). Hence, yield versus time data provide the same kinetics parameters as in the case that concentrations would be considered. The same reasoning holds for the other 2 cases, see Sections 2.2 and 2.3.

It should be noted that the provided estimation tool (see Supplementary Materials) is also capable of handling reaction orders other than unity.

Experimental data, reported as conversion and selectivity, were taken from the paper [34]. They were transformed into yield data, with yield = conversion x selectivity. The authors studied three systems of colloids: polyvinylpyrrolidone-protected Ag^0 clusters in N,N-dimethylacetamide (DMA) and Co^0 clusters in N,N-dimethylformamide (DMF), respectively denoted as Ag^0/DMA and Co^0/DMF. These systems showed superior catalytic activity compared to the colloids in alcohol solutions; mainly due to the suppression of aldol side reactions. In order to make sure that the metal colloids are fully reduced at the start of the reaction, the Ag^0/DMA sol system was also reduced by a priori pressurization at 2.0 MPa H_2 at 298 K for 1 h; this system is denoted as Ag^0/DMA*.

2.2. Hydrogenation of Cinnamaldehyde

A second example in the selective hydrogenation of α,β-unsaturated aldehydes is the hydrogenation of cinnamaldehyde (CAL), which produces useful unsaturated intermediates including C=O hydrogenated cinnamyl alcohol (COL) and C=C hydrogenated hydrocinnamic aldehyde (HCAL) for pharmaceutical and fragrance applications [38]. COL and HCAL can further be hydrogenated to hydrocinnamic alcohol (HCOL), see Scheme 2. In this example, Zhu et al. [35] reported a class of products as 'others'. Therefore, all com-

pounds are assumed in this work to be eligible to react are lumped into product Q. In other words, all measurable compounds—namely reactant CAL and products COL (desired), HCAL, and HCOL—are assumed to undergo subsequent (unspecified) reactions 6 to 9. Since these products are not individually quantified, they are collectively represented as a single compound, Q. This approximation does not affect the kinetic parameters for the primary reactions of interest (reactions 1 through 5). Conversely, the transformation of the measurable compounds into unquantified products can be described using reaction coefficients k_6 to k_9, based on the available experimental data.

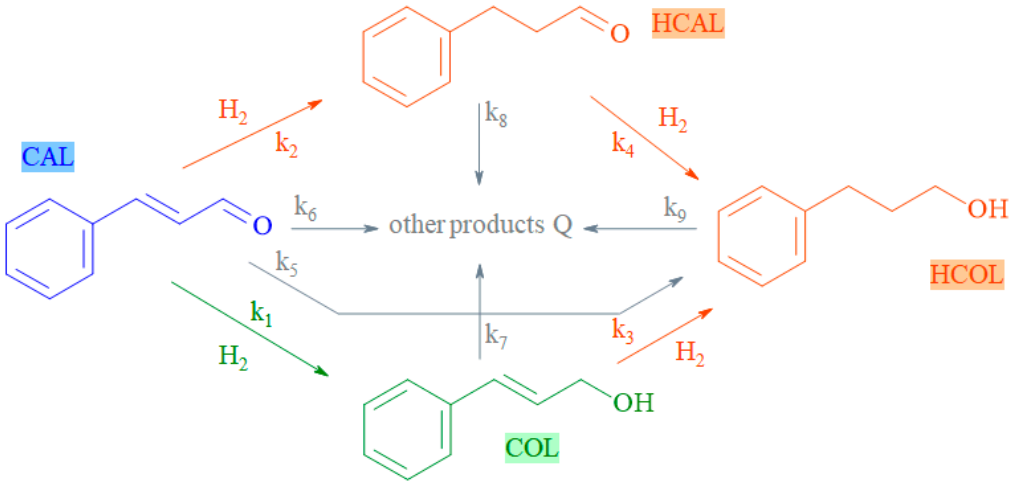

Scheme 2. Reaction of cinnamaldehyde (CAL) into cinnamyl alcohol (COL), hydrocinnamic aldehyde (HCAL), hydrocinnamic alcohol (HCOL) and other products (Q). Additional grey reaction arrows are added to the scheme presented by Zhu et al. [35].

All reactions are considered to be first-order, with reaction coefficient k_1 to k_4. Direct hydrogenation into HCOL is governed by reaction coefficient k_5. The formation of undesired reaction products (others), which are lumped into Q, is modeled via first-order consecutive reactions for CAL, HCAL, COL and HCOL with reaction coefficients k_6 to k_9:

$$\frac{dC_{CAL}}{dt} = -k_1 C_{CAL} - k_2 C_{CAL} - k_5 C_{CAL} - k_6 C_{CAL} \quad (9)$$

$$\frac{dC_{COL}}{dt} = k_1 C_{CAL} - k_3 C_{COL} - k_7 C_{COL} \quad (10)$$

$$\frac{dC_{HCAL}}{dt} = k_2 C_{CAL} - k_4 C_{HCAL} - k_8 C_{HCAL} \quad (11)$$

$$\frac{dC_{HCOL}}{dt} = k_3 C_{COL} + k_4 C_{HCAL} + k_5 C_{CAL} - k_9 C_{HCOL} \quad (12)$$

$$\frac{dC_Q}{dt} = k_6 C_{CAL} + k_7 C_{COL} + k_8 C_{HCAL} + k_9 C_{HCOL} \quad (13)$$

$$(C_{CAL})_{t=0} = C_{CAL,0} \quad (14)$$

$$(C_{HCAL})_{t=0} = (C_{COL})_{t=0} = (C_{HCOL})_{t=0} = (C_Q)_{t=0} = 0 \quad (15)$$

Integration of Equations (9)–(13) with initial conditions (14) and (15) gives the time-dependent functions for the corresponding concentration values of CAL, COL, HCAL, HCOL and Q, see Section S.4 of the Supplementary Materials for corresponding closed form expressions.

In order to perform the CAL hydrogenation reaction, Zhu et al. [35] prepared supported Pd catalysts on carbon nanotubes (CNTs). Catalysts Pd/CNT-PNIPAM (L), Pd/CNT-PNIPAM (H) and Pd/CNT-PNIPAM (LH) were synthesized by the impregnation–reduction

of Pd onto a CNT-PNIPAM hybrid material, made by grafting of N-isopropylacrylamide (NIPAM) onto CNT-A material. Extensions 'L', 'H' and 'LH' respectively denote preparation treatment at low temperature (25 °C), high temperature (50 °C) and mixed temperatures (25 and 50 °C). The major reasoning for the difference in synthesis was the lower critical solution temperature (LCST) of 32 °C, so that in the 'L' catalyst the Pd deposition was mainly on the hydrophilic side chain of PNIPAM and that the 'H' catalyst showed Pd deposition on the backbone of surface PNIPAM coils. The 'LH' catalyst showed Pd deposition on the backbone as well as inside the PNIPAM coils due to structural transformation of the PNIPAM. Reduction also took place partially at 25 and 50 °C.

For comparison, CNT and CNT-A (after surface acidification with a 3:1 H_2SO_4:H_2O_2 solution) supported Pd were also prepared by the authors [35]. The latter has typically grafted hydroxyl groups on its surface.

2.3. Hydrogenation of Dicyclopentadiene

Endo-tetrahydrodicyclopentadiene (THDCPD) is not only a high-energy-density solid fuel but also an important intermediate for the synthesis of *exo*-tetrahydrodicyclopentadiene [40,41]. Generally, THDCPD is synthesized by the hydrogenation of dicyclopentadiene (DCPD), which is separated from the C5 by-product of the naphtha pyrolysis process [42]. Fang et al. [36] propose a reaction scheme with 8,9-dihydrocyclopentadiene as a hydrogenation intermediate as given in Scheme 3, with corresponding CE (16) to (19):

$$\frac{dC_{DCPD}}{dt} = -k_1 C_{DCPD} - k_3 C_{DCPD} - k_5 C_{DCPD} + k_4 C_D^2 \quad (16)$$

$$\frac{dC_{8,9-DHDCPD}}{dt} = k_1 C_{DCPD} - k_2 C_{8,9-DHDCPD} \quad (17)$$

$$\frac{dC_{DHDCPD}}{dt} = k_2 C_{8,9-DHDCPD} + k_5 C_{DCPD} \quad (18)$$

$$\frac{dC_D}{dt} = 2k_3 C_{DCPD} - 2k_4 C_D^2 \quad (19)$$

$$(C_{DCPD})_{t=0} = C_{DCPD,0} \quad (20)$$

$$(C_{8,9-DHDCPD})_{t=0} = (C_{THDCPD})_{t=0} = (C_D)_{t=0} = 0 \quad (21)$$

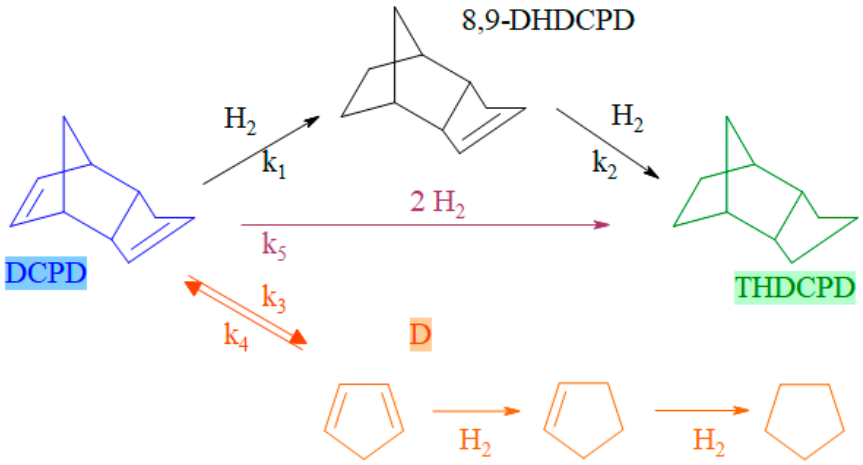

Scheme 3. Reaction scheme for hydrogenation of dicyclopentadiene (DCPD) into 8,9-dihydrocyclopentadiene (8,9-DHDCPD), *endo*-tetrahydrodicyclopentadiene (THDCPD) and lumped C5 fraction with cyclopentadiene, cyclopentene and cyclopentane (D) [36] with additional grey arrow proposed in this work.

Analytical integration of Equations (16)–(19) with initial conditions (20) and (21) is only possible if $k_4 = 0$ (secondary order reaction). In this case, the time-dependent functions for the corresponding concentration values of DCPD, 8,9-DHDCPD, THDCPD and D are given in Section S.5 of the Supplementary Materials.

Fang et al. [36] prepared a series of $NiMo_x/\gamma\text{-}Al_2O_3$ (x = 0, 0.02, 0.05, 0.10, 0.20 and 0.50) bimetallic catalysts via the incipient wetness co-impregnation method and they investigated the influence of Mo on the performance of DCPD hydrogenation. In the current study, the catalysts with x = 0.05, 0.10, 0.20, and 0.50 are investigated, as the surface atomic composition can be significantly determined from reported XPS data. Consequently, the set of kinetic parameters obtained can be correlated with the structural properties of the different catalysts.

2.4. Parameter Estimation

In order to keep the focus on its application, the details on the integration of the CE and subsequent parameter estimation via the proposed tool, which is written in an accessible Excel® format (Microsoft 365), can be found in Section S.6 of the Supplementary Materials. Confidence intervals for 95% certainty are calculated using the calculated covariance matrix (derivatives are numerically evaluated) as described in references [1,43]. When the latter surpasses the actual parameter value, the associated parameter is considered non-significant and should be set to zero. If multiple parameters are deemed non-significant, the one with the largest standard deviation is set to zero, and the process is repeated. In other words, after removing one parameter, the remaining parameters in the simplified model must be re-estimated. Removing a non-significant parameter should not cause substantial changes to the other parameters [1,2]. The results were cross-checked by ODR Pack, which is a regression package used in previous research [44–47] and the same results were obtained. Some guidelines how to use the tool are provided in Sections S.7 and S.8 of the Supplementary Materials containing the comparison of currently existing Excel® tools for kinetic modeling with the tool proposed in this work.

2.5. Remark on Experimental Conditions

In order to guarantee a constant hydrogen concentration in the liquid phase, which is tacitly considered in all reaction terms in Sections 2.1–2.3, it is important the check the experimental details. For example, Zhu et al. [35] explicitly mention in their paper that the hydrogen headspace is continuously replenished. In other literature examples, the ratio of initial concentrations of hydrogen to substrate is substantially higher than unity [5,37], which guarantees (at not too high conversion) a near constant hydrogen concentration in the solvent.

It is also advised to check the quantitative criterion for the liquid-phase hydrogenation reactions described by Ramachandran and Chaudhari to analyze the significance of gas–liquid, liquid–solid and intraparticle mass transfer on the reaction kinetics [3,48].

3. Results

For the first example, Mertens et al. [34] report data versus time for citral hydrogenation into the corresponding allyl alcohol ((2E)-3,7-dimethylocta-2,6-dien-1-ol), which is the compound of interest with the reaction scheme given in Scheme 1. The experimental data (from the original paper) and calculated responses (in this work) can be found in Figure 1.

Regarding the reaction scheme and the corresponding CE (3) to (6), parameters k_3 and k_4 could not be significantly estimated for the three catalyst systems, which means that both direct conversion of citral (CAL) and conversion of the allyl alcohol (AA) into other products than single hydrogenated compounds can be excluded over the given systems.

From this observation, it can be concluded that all metal sol catalysts are selective towards direct hydrogenation in general.

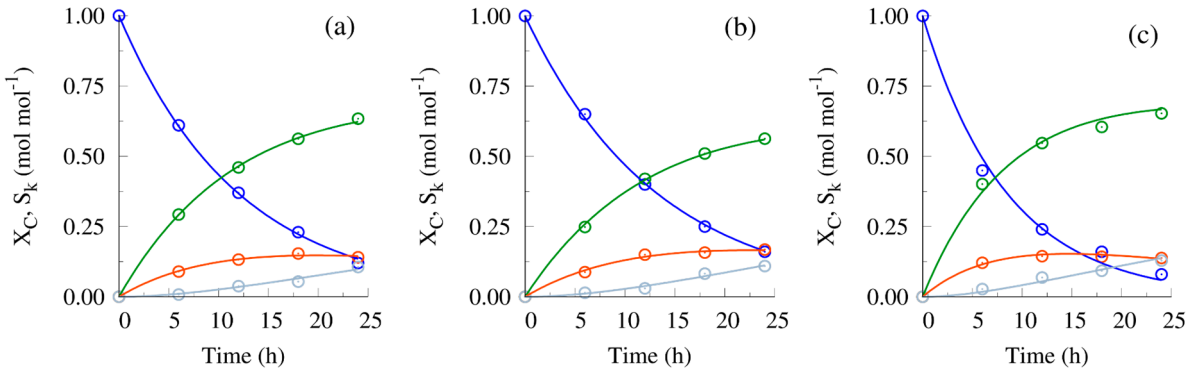

Figure 1. Experimental conversion of citral (○) and selectivity towards the corresponding allyl alcohol (○), citronellal (○), and other products (○), according to Scheme 1. (**a**) Ag^0/DMA, (**b**) Co^0/DMF and (**c**) Ag^0/DMA after pretreatment by pressurization to 2.0 MPa at 298 K for 1 h. Conditions: citral:catalyst = 200 mol mol^{-1}, P = 2.0 MPa and T = 298 K [34]. Full lines are calculated via integration of Equations (3)–(6) with initial conditions (7) and (8) and kinetic parameters, reported in Table 1.

Table 1. Parameter estimates in citral hydrogenation over Ag^0 and Co^0 nanocolloids; $|e|_{max}$ represents maximal deviation between experimental data, after [34] and modeled data.

System	Ag^0/DMA	Co^0/DMF	Ag^0/DMA*
k_1 (h^{-1})	$(6.07 \pm 0.42)\cdot10^{-2}$	$(5.16 \pm 0.40)\cdot10^{-2}$	$(8.47 \pm 1.13)\cdot10^{-2}$
k_2 (h^{-1})	$(2.28 \pm 0.21)\cdot10^{-2}$	$(2.39 \pm 0.24)\cdot10^{-2}$	$(3.28 \pm 0.53)\cdot10^{-2}$
k_5 (h^{-1})	$(3.44 \pm 0.56)\cdot10^{-2}$	$(3.56 \pm 0.61)\cdot10^{-2}$	$(4.39 \pm 1.02)\cdot10^{-2}$
RSSQ	$3.59\cdot10^{-3}$	$4.67\cdot10^{-3}$	$1.17\cdot10^{-2}$
$\|e\|_{max}$	$1.51\cdot10^{-2}$	$1.56\cdot10^{-2}$	$4.40\cdot10^{-2}$
ρ_{max}	0.376 (k_1 and k_2)	0.355 (k_1 and k_2)	0.540 (k_1 and k_2)

Values for the significant parameter estimates are mentioned in Table 1, from which it is clear that the Ag^0/DMA system shows an AA formation reaction coefficient k_1 which is ~18% higher compared to the Co^0/DMF system. In both systems, citronellal (CN) formation shows no significant difference (parameter k_2). A similar observation can be made for parameter k_5: there is no significant difference in the systems for the further reaction of citronellal. It is important to notice that the AA formation is significantly different in both systems, whereas further reactions are rather comparable and this observation cannot be made from conversion–selectivity data alone.

The ratio k_1/k_2 can be considered as a measure for the AA selectivity: for system Ag^0/DMA the value 2.7 ± 0.19 is obtained, whereas 2.2 ± 0.17 is calculated for the Co^0/DMF system. Upon inspection of Scheme 1, the selectivity towards the desired product (2E)-3,7-dimethylocta-2,6-dien-1-ol (or AA) is calculated as $k_1/(k_1 + k_2 + k_3)$. Since k_3 cannot be significantly estimated, the selectivity towards the desired product is given by the ratio $k_1/(k_1 + k_2)$. In this respect, the ratio k_1/k_2 is a measure for the selectivity, but it does not represent the selectivity as such. If this ratio is defined as β, the actual selectivity can be calculated as $k_1/(k_1 + k_2) = (k_1/k_2)/((k_1/k_2) + 1) = \beta/(1 + \beta)$. For the given catalysts (with β value of 2.7 ± 0.19 and 2.2 ± 0.17), the selectivity is calculated as 0.73 ± 0.05 and 0.69 ± 0.05 for the Ag^0/DMA and Co^0/DMF system, respectively. This corresponds well with the experimentally reported values of 0.72–0.75 mol/mol and 0.67–0.71 mol/mol for the Ag^0/DMA and Co^0/DMF system, respectively [34].

In a comparison between the Ag^0/DMA as such and the Ag^0/DMA*, it can be observed from Table 1 that all reaction coefficients are higher after prereduction of the catalyst. Moreover, it can be noticed that coefficients k_1 and k_2, responsible for the direct citral conversion, respectively differ by a factor of 1.40 ± 0.21 and 1.44 ± 0.27. Hence, the catalyst pretreatment results in a simultaneous increase in the desired and undesired reaction rate, which corresponds to the similar experimentally observed selectivity. Indeed, the higher experimental conversion without change in selectivity, i.e., the ratio $k_1/(k_1 + k_2)$, does not significantly change, but the absolute value of $k_1 + k_2$ increases.

Regarding previous experimental results, a suggestion for future experimental work can be the synthesis of a series of prereduced catalysts, whereby the reduction time or temperatures vary. The proposed methodology in this paper can be applied to extract kinetic coefficients and the synthesis effects can be related to the kinetic reaction rates and kinetic parameters for the individual considered reactions.

In conclusion, for the first example, it can be noted that the obtained results could not be extracted from conversion–selectivity data only, but specific parameter estimation is required. Importantly, due to the parameter estimation it can be revealed that prereduction gives rise to a simultaneous increase in reaction rate coefficients.

In the reaction scheme for the second example, the single hydrogenation of CAL into COL and HCAL with subsequent hydrogenation into HCOL are included. However, when the reported data are inspected, the HCOL selectivity versus CAL conversion does not seem to pass the origin (these graphs are mentioned in the original paper: Figure 10, p. 18, [35]), which means that there should also be a direct route of double hydrogenation included in the scheme. This is represented by reaction with coefficient k_5. Also, the authors report 'others' as undefined products. This is accounted for in this work by putting forward that all of the compounds in the scheme can further react into undesired products, lumped into one 'other' concentration, Q, corresponding to reactions with coefficients k_6 to k_9.

Figure 2 shows experimental values for CAL conversion and product yields for the Pd/CNT-PNIPAM catalysts, taken from conversion and selectivity data reported in [35]. For all five catalytic systems reaction coefficients k_3, k_7, k_8 and k_9 could not significantly be estimated. This corresponds to the fact that (1) the reported data do not support the consecutive reaction of COL, the desired product, into HCOL and that (2) compounds CAL, COL and HCOL do not significantly contribute to the formation of 'other' products based on the given experimental data. This can probably be explained by the small response for other products.

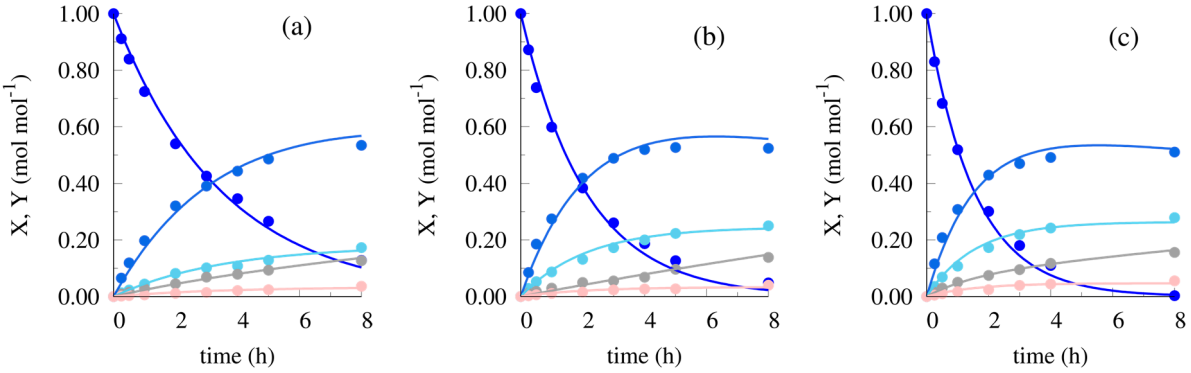

Figure 2. Experimental conversion of CAL (•) and selectivity towards HCAL (•), COL (•), HCOL (•) and other products (•) over catalyst Pd/CNT-PNIPAM (L) (**a**), Pd/CNT-PNIPAM (H) (**b**) and Pd/CNT-PNIPAM (LH) (**c**). Conditions: 0.2 gcat and 2.0 g CAL, P = 3.0 MPa and T = 353 K [35]. Full lines are calculated via integration of Equations (9)–(13) with initial conditions (14) and (15) and kinetic parameters, reported in Table 2.

Table 2. Parameter estimates in cinnamaldehyde hydrogenation over thermo-responsive polymer grafted carbon nanotubes; $|e|_{max}$ represents maximal deviation between experimental data, after [35], and modeled data.

System	Pd-CNT	Pd-CNT (A)	Pd/CNT-PNIPAM (L)	Pd/CNT-PNIPAM (H)	Pd/CNT-PNIPAM (LH)
k_1 (h^{-1})	$(6.47 \pm 0.58)\cdot10^{-2}$	$(1.01 \pm 0.16)\cdot10^{-1}$	$(5.15 \pm 0.66)\cdot10^{-2}$	$(1.16 \pm 0.15)\cdot10^{-1}$	$(1.70 \pm 0.24)\cdot10^{-1}$
k_2 (h^{-1})	$(1.53 \pm 0.12)\cdot10^{-1}$	$(3.41 \pm 0.46)\cdot10^{-1}$	$(1.98 \pm 0.18)\cdot10^{-1}$	$(3.21 \pm 0.33)\cdot10^{-1}$	$(3.86 \pm 0.47)\cdot10^{-1}$
k_4 (h^{-1})	$(2.34 \pm 1.57)\cdot10^{-2}$	$(6.87 \pm 2.85)\cdot10^{-2}$	$(1.78 \pm 1.60)\cdot10^{-2}$	$(2.87 \pm 1.58)\cdot10^{-2}$	$(2.03 \pm 1.61)\cdot10^{-2}$
k_5 (h^{-1})	$(1.10 \pm 0.85)\cdot10^{-2}$	$(6.09 \pm 3.52)\cdot10^{-2}$	$(2.52 \pm 1.14)\cdot10^{-2}$	$(2.08 \pm 1.83)\cdot10^{-2}$	$(5.90 \pm 2.43)\cdot10^{-2}$
k_6 (h^{-1})	$(6.48 \pm 1.74)\cdot10^{-3}$	$(2.34 \pm 0.70)\cdot10^{-2}$	$(9.56 \pm 2.84)\cdot10^{-3}$	$(1.58 \pm 0.50)\cdot10^{-2}$	$(3.04 \pm 0.87)\cdot10^{-2}$
RSSQ	$1.83\cdot10^{-2}$	$4.63\cdot10^{-2}$	$1.97\cdot10^{-2}$	$2.86\cdot10^{-2}$	$2.65\cdot10^{-2}$
$\|e\|_{max}$	$4.34\cdot10^{-2}$	$6.55\cdot10^{-2}$	$3.62\cdot10^{-2}$	$5.80\cdot10^{-2}$	$5.08\cdot10^{-2}$
ρ_{max}	-0.919 (k_4 and k_5)	-0.875 (k_4 and k_5)	-0.882 (k_4 and k_5)	-0.867 (k_4 and k_5)	-0.793 (k_4 and k_5)

The parameter estimates are collected in Table 2. From the first comparison between Pd/CNT and Pd/CNT-A, it can be observed that all parameter values are higher on the latter catalyst and, especially, the value for k_5 differs by a factor of 5.5, which explains the lower selectivity towards COL when acidified CNTs are used. From the given parameter values, the initial selectivity is calculated as the ratio of k_1 to the sum of k_1, k_2, k_5 and k_6. This gives respectively the values of 0.275 ± 0.025 mol mol^{-1} and 0.193 ± 0.033 mol mol^{-1}. Experimental COL selectivity values for $X_{CAL} < 0.60$ mol mol^{-1} are reported to be 0.242 mol mol^{-1} and 0.158 mol mol^{-1}, which satisfactorily align with the calculated values. In conclusion, it appears that the surface acidification is not beneficial for this application, since the undesired reactions (2, 5 and 6) proceed faster, compared to the desired one, corresponding to k_1, giving overall lower selectivity to COL.

Comparison of the PNIPAM-based catalysts Pd/CNT-PNIPAM (L), Pd/CNT-PNIPAM (H) and Pd/CNT-PNIPAM (LH) with respect to COL selectivity gives 0.181 ± 0.020, 0.245 ± 0.026 and 0.264 ± 0.047 mol mol^{-1}. This signifies that the catalyst with intermediate treatment shows the highest selectivity, which can probably be assigned to the higher extent of initial Pd reduction or the specific synthesis method. This conclusion corresponds to the previously addressed results in the work of Mertens et al. [34]. However, both H and LH treatments can be considered to have similar selectivity if the standard deviation is taken into account.

Referring to the synthesis method of the Pd catalysts, the authors of the original paper [35] reported in their paper that if the solvent temperature (for catalyst synthesis) is below the lower critical solution temperature (LCST) at about 32 °C, this gives a hydrophilic surface for the carbon nanotube; while it curls to a compressed coil if ambient temperature ascends to above LCST, resulting in a hydrophobic one. This different temperature for catalyst synthesis has a clear effect on the Pd deposition as the Pd dispersion was reported in the original paper as $34.9 \pm 7.8\%$, $27.9 \pm 6.4\%$ and $30.8 \pm 4.7\%$ for the Pd/CNT-PNIPAM (H), Pd/PNIPAM (H) and Pd/CNT-PNIPAM (LH) catalysts, respectively.

In a specific comparison between the low- and high-temperature treatment catalysts Pd/CNT-PNIPAM (L) and Pd/CNT-PNIPAM (H), it can be observed from the estimated parameters in Table 2 that single hydrogenation reactions 1, 2 and 4 show more or less a doubling of the reaction coefficient (factor 1.8 ± 0.4). For reaction 5 a comparable and for reaction 6 a slightly higher reaction coefficient value is obtained.

All of the reaction coefficient values (except k_4) for the Pd/CNT-PNIPAM (LH) catalyst are higher than for the catalysts Pd/CNT-PNIPAM (L) and Pd/CNT-PNIPAM (H). Especially, the double hydrogenation coefficient k_5 is ~2.5 times higher. From a catalyst design point of view, it could be suggested that catalysts can be prepared with intermediate temperature reduction treatment so that higher COL selectivity can be obtained by, for

example, suppressing this double hydrogenation. This can be directly linked to the specific nature of the active sites and their spatial morphology on the catalyst surface, as it appears on the PNIPAM backbone and inside the PNIPAM coils [35]. Especially, the temperature treatment of the different catalysts gives rise to a different Pd dispersion, as reported in the original paper [35]: 34.9 ± 7.8%, 27.9 ± 6.4% and 30.8 ± 4.7% for the Pd/CNT-PNIPAM (H), Pd/PNIPAM (H) and Pd/CNT-PNIPAM (LH) catalysts, respectively. When one inspects the value for k_1 (Table 2), which corresponds to the desired reaction for the conversion of CAL into COL, an intermediate dispersion gives the highest rate coefficient (an example of a structure–activity relation). Unfortunately, k_5 also increases accordingly, so it is advisable to investigate more treatment temperatures to find out optimal kinetics (high k_1, low k_5), if possible, as was suggested for the other examples in this paper.

Closing the second example, it can be mentioned that, without specific modeling and corresponding parameter estimation, the given conclusions could have never been made, so catalyst preparation, proposition of reaction mechanism and validation by modeling are crucial for optimization of catalytic materials in order to optimize desired compound selectivity.

Additionally, regarding previous experimental results, a suggestion for future experimental work can be the synthesis and the usage of a series of catalysts for the same reaction. The methodology presented in this paper can be applied to extract kinetic coefficients, enabling the investigation of how different catalysts and synthesis conditions influence the corresponding reaction kinetics. Combining this approach with an analysis of the experimental product distribution can provide valuable insights into the material synthesis, allowing for a deeper understanding of the relationship between synthesis parameters, product outcomes, and the kinetic behavior of the individual reactions.

The third example considers the DHDP hydrogenation over a $NiMo_x/\gamma\text{-}Al_2O_3$ catalyst (x = 0.05, 0.10, 0.20 and 0.50) and application of the model in Section 2.3 gives kinetic parameters as reported in Table 3. The original scheme in reference [36] reports an equilibrium between the dicyclopentadiene and D, representing lumped concentrations of cyclopentadiene, cyclopentene and cyclopentane, but in all cases the coefficient for the reversible step could not be significantly estimated. This leads to the conclusion that the formation of D should be considered to happen in an irreversible mode which can probably be explained by the reported low yield for D (<0.02 mol mol^{-1}) [36].

Table 3. Parameter estimates in DCPD hydrogenation over catalyst $NiMo_x/\gamma\text{-}Al_2O_3$ (x = 0.05, 0.10, 0.20 and 0.50); $|e|_{max}$ represents maximal deviation between experimental data, after [36], and modelled data. The value Mo/Ni is based on the surface atomic composition (atomic %) for Mo and Ni for the different compositions x. (1) Could not be estimated significantly.

x	0.05	0.10	0.20	0.50
Mo/Ni	0.04	0.14	0.23	0.54
k_1 (h^{-1})	$(8.58 \pm 1.33)\cdot10^{-1}$	$(6.42 \pm 3.31)\cdot10^{-1}$	$(7.91 \pm 4.45)\cdot10^{-1}$	$(1.09 \pm 0.13)\cdot10^{+0}$
k_2 (h^{-1})	$(2.79 \pm 0.63)\cdot10^{+0}$	$(2.31 \pm 1.20)\cdot10^{+0}$	$(2.62 \pm 1.38)\cdot10^{+0}$	$(3.28 \pm 0.53)\cdot10^{-2}$
k_3 (h^{-1})	$(3.73 \pm 2.32)\cdot10^{-3}$	$(3.23 \pm 0.97)\cdot10^{-3}$	$(3.11 \pm 0.82)\cdot10^{-3}$	$(3.28 \pm 0.53)\cdot10^{-2}$
k_5 (h^{-1})	- (1)	$(4.43 \pm 1.75)\cdot10^{-1}$	$(6.47 \pm 4.68)\cdot10^{-1}$	- (1)
RSSQ	$2.65\cdot10^{-2}$	$4.67\cdot10^{-3}$	$2.32\cdot10^{-2}$	$1.20\cdot10^{-2}$
$\|e\|_{max}$	$7.01\cdot10^{-2}$	$2.28\cdot10^{-2}$	$2.68\cdot10^{-2}$	$5.33\cdot10^{-2}$
ρ_{max}	0.214 (k_1 and k_2)	0.976 (k_2 and k_5)	−0.984 (k_2 and k_5)	0.218 (k_1 and k_3)

Figure 3a gives the results for the $NiMo_{0.20}/\gamma\text{-}Al_2O_3$ catalysts, which were considered to have the optimal composition regarding the Mo addition. After ~3 h the intermediate 8,9-DHDCPD is fully converted into the desired THDCPD, and since the reported yield of

single 5-ring compounds is very low, it can be concluded that almost 100% selectivity is obtained over the given catalysts.

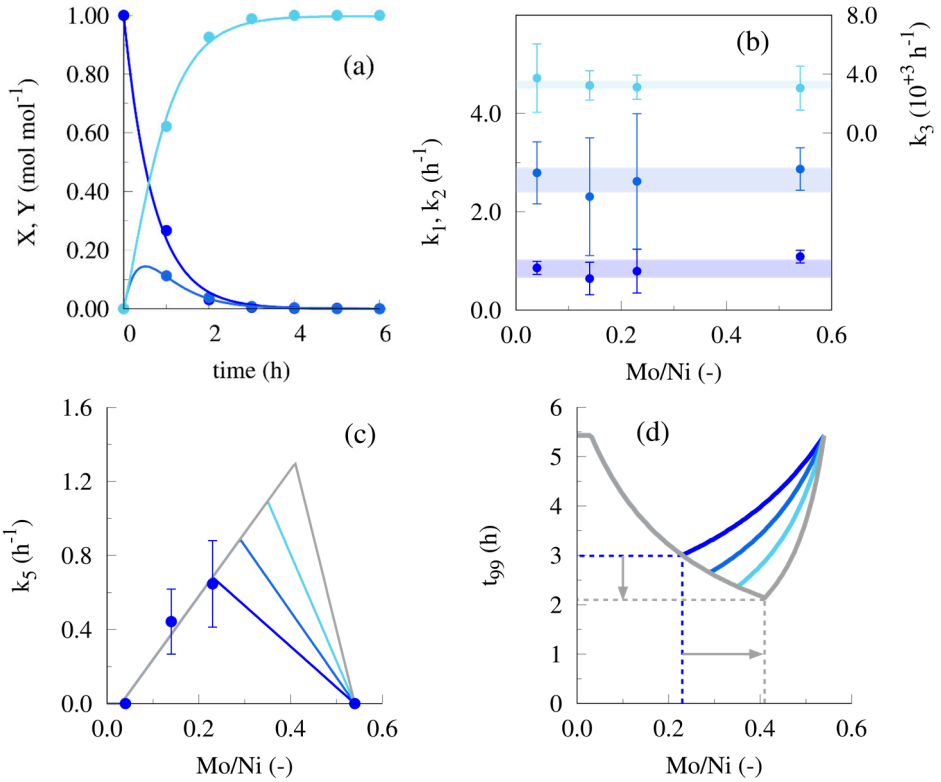

Figure 3. (**a**) DCPD conversion (●) and yield of 8,9-DHDCPD (●) and THDCPD (●) over $NiMo_{0.20}/\gamma$-Al_2O_3 catalysts. Conditions: 0.5 g prereduced catalyst, 5 g DPCD, 50 g cyclohexane as solvent, P = 3.5 MPa and T = 423 K. Full lines are calculated via integration of Equations (16)–(19) with initial conditions (20) and (21) and parameter estimates reported in Table 3. (**b**) Reaction coefficients k_1 (●), k_2 (●) and k_3 (●) with colored band representing average ± standard deviation. (**c**) Structure–reactivity relation for reaction coefficients k_5 (●) and proposed optimal compositions Mo/Ni = 0.23 (▬), 0.29 (▬), 0.35 (▬) and 0.41 (▬); and (**d**) corresponding reaction time to reach 0.99 mol mol^{-1} conversion.

From Table 3 it can be observed that subsequent single hydrogenation reaction coefficients are not significantly different with regard to the Mo/Ni ratio, which is graphically represented in Figure 3b (k_1 and k_2 on the left axis and k_3 on the right axis). In order to double check this observation, statistical analysis showed that a linear fit resulted in a non-significant slope and, hence, the parameters do not depend on the specific composition.

The direct double hydrogenation, with reaction coefficient k_5, is proposed to be added to the reaction scheme of the original paper, see Scheme 3. The rationale is that the corresponding simultaneous adsorption of both double bonds can also occur on the catalyst surface, as was proposed in the original paper [36]. For this parameter k_5 some interesting observations can be drawn: for the lowest Mo/Ni ratio, corresponding to catalyst $NiMo_{0.05}/\gamma$-Al_2O_3, parameter k_5 could not be estimated significantly. In mechanistic terms this corresponds to the fact that the double hydrogenation does not significantly take place and it should be set to zero. Probably, the corresponding low Mo surface coverage does not offer suitable or just not enough (couples of) active sites to this reaction. However, an increase in k_5 value is observed for increasing Mo/Ni value, up to (6.47 ± 4.68) 10−1 h−1, but for the highest reported value (x = 0.50) it shows the value (2.04 ± 7.30) 10−3 h−1, so it has to be considered statistically not different from 0. From the given results, it can be

suggested that an intermediate composition (between x = 0.20 and 0.50) might result in an even higher conversion with a corresponding increase in yield in a shorter reaction time.

In the original paper, a decrease for Ni average particle size was observed from XRD data, until no peak was visible, which occurred for x = 0.20. It was concluded that metallic aggregation was restrained by adding Mo species. Further, the catalyst reducibility was investigated by H_2-TPR and with an increasing Mo content the relative content of well-dispersed NiO also increased, proven by a decrease in reduction peak data. The presence of Mo^{4+} was conjectured to play a key role in the catalysis process and, after taking into account the data from the Supplementary Materials in reference [36], it was reported that the relative area for the $Mo^{4+} \rightarrow Mo^0$ reduction peak increased with increasing x value but that the lowest reduction temperature was found at x = 0.20. This can suggest that a particular organization of surface atoms was beneficial for the double hydrogenation reaction with regard to specific adsorption mode and from the tested values, x = 0.02, 0.05, 0.10, 0.20 and 0.50, it appeared that x = 0.20 resulted in the best catalytic performance. This corresponds to the earlier observation that the double hydrogenation coefficient (k_5), obtained from reported experimental data, is the highest at x = 0.20, while the other hydrogenation coefficients are more or less equal, independent of the composition.

Figure 3c shows that parameter k_5 is not significantly different from 0 for low and high x values and it displays the highest value for the intermediate value of x = 0.20, which suggests a structure–reactivity relation. From this observation the question arises whether a possible composition, other than the experimentally tested ones, with $0.20 \leq x \leq 0.50$ and corresponding $0.23 \leq Mo/Ni \leq 0.54$, could lead to an even better catalytic activity. To this end, simulations with Mo/Ni = 0.23 + 0.06·k and k = 1…3 are performed, from which it can be observed that the total reaction time can be reduced from ~3 h to ~2 h, see Figure 3d. From an engineering point of view, it is of interest to synthesize and test the intermediate compositions, since this improvement can eventually lead to a production increase of ~33%.

Taking everything into account in the third example, based on an initial set of compositions for catalyst synthesis, a combination of experimental techniques such as physical characterization (XRD, XPS…) and chemical characterization (H_2-TPR and reaction data), intermediate compositions could be prepared and they can be tested to check the suggested superior activity and performance.

After the discussion of the given examples, it is worthwhile to mention that the maximal deviation of experimental data and calculated data, $|e|_{max}$, is ~7%, see Table 3, so that the pseudo-homogeneous models can be considered to describe the experimental data quite precisely and, as such, that the model parameters can be used for optimization of related synthesis procedures. The 'best' catalyst can then always be evaluated by more experimental data and a more thorough kinetic modeling, e.g., based on elementary reaction steps. At the end of the day, it is always advisable to perform thorough kinetic modeling using a substantial experimental data set, but this is not always possible due to a lack of data of time for modeling and, in this matter, the proposed tool can provide user-friendly help in possible catalyst optimization.

At the end of this section it is important to note that the proposed approach does not include adsorption and corresponding adsorption terms in reaction rate expressions are not taken up, as it is common to model hydrogenation reactions as such [3,5–7,37]. In addition, this inclusion would require an approach in calculation that is different from that presented in the current tool (see Supplementary Materials). This is part of future work, where other types of reactions, e.g., heterogeneously catalysed oxidation reactions, can be evaluated. On the other hand, the modeling of this type of selective oxidation reaction can also be done by the proposed approach, especially when equilibrium is not assumed and

the forward adsorption and backward desorption are taken into account. Examples are the study of the (gas-phase) ethane oxidation over $MoVTeNbO_x$ [49] and the kinetic study of cyclohexane oxidation reaction in gas phase over the catalyst $20FeMnO_\delta$/(3CeAl) [50]. Other examples involving a solid catalyst using a similar modeling approach (as used in this work) can be found in the literature, e.g., (1) the study of the hydrolytic kinetic resolution catalysed by a (salen)-Co(III) complex for the preparation of highly enantio-enriched terminal epoxides [51], (2) the one-pot hydrogenolysis of cellulose to glycols over a $Ru@Fe_3O_4$/polymer catalyst [52], (3) the study of glycerol hydrogenolysis to produce bio-propanol over a Ni/C catalyst modified with $Al(H_2PO_4)_3$ [53], or (4) the investigation of the toluene alkylation over Y-type zeolite catalysts [54].

A second remark is that the purpose of this work to not to evaluate data for Arrhenius parameters, but it is to link the composition, or differences in synthesis method, showing how exactly conversion and yield values are altered. Once the highest conversion (or yield) is determined, between the distinct points, full kinetic modeling can be undertaken with the inclusion of adsorption terms with isothermal kinetic analysis at first, followed by non-isothermal kinetic regression.

The key takeaway from this manuscript is that the specific kinetic parameters, whether obtained through simple methods (as presented here) or comprehensive kinetic data analysis (for each synthesized catalyst), must always be correlated with catalyst descriptors, such as active sites. The first approach can be performed in just a few minutes (for quick screening) using the provided Excel® file, while the latter requires more time due to experimental performance and kinetic analysis. Especially, when one has the possibility to perform catalytic reactions in high-throughput systems [55] or catalytic hybrid nanoreactors with fast catalyst preparation [56], several catalysts (with different synthesis) can be evaluated and the obtained kinetic parameters can be linked to the synthesis details and, hence, one can establish structure–activity relations. These are very important in catalysis to understand the optimal product distribution for a given reaction and starting reactant.

Finally, the authors would like to clarify that the catalytic data used in this manuscript are solely for illustrative purposes; the previously reported work on catalyst properties is neither discussed nor modified. This contribution should be viewed as an extension of those earlier excellent reports, where experimental results and kinetics are integrated. The reason for selecting these particular examples was that the cited papers reported both conversion and selectivity data for hydrogenation reactions.

4. Conclusions

This work offers several examples demonstrating how data collected from hydrogenation experiments can be leveraged to derive kinetic insights, which can then guide subsequent catalyst development or enhance the interpretation of the results. More precisely, this manuscript shows that the combination of (1) the estimation of kinetic parameters, (2) physical characterization, using typical XRD, XPS... data and (3) chemical characterization such as H_2-TPR together with can be helpful in the elucidation of proposed reaction schemes regarding the significance of included steps and it can have potential to help in catalyst design with possible superior activity regarding conversion and selectivity. Hydrogenation reactions of citral, cinnamaldehyde and dicyclopentadiene are taken to showcase the applicability of an Excel® tool, provided in this work, which is able to estimate kinetic parameters in a matter of minutes (afterwards the best catalyst can be fully modelled using appropriate adsorption terms and temperature Arrhenius dependencies).

Supplementary Materials: The following supporting information can be downloaded at: https://www.mdpi.com/article/10.3390/reactions7030041/s1, Figure S1: DCPD conversion (●) and yield of 8,9-DHDCPD (●) and THDCPD (●) over $NiMo_x/\gamma$-Al_2O_3 catalysts with (a) x = 0.05, (b) x = 0.10, (c) x = 0.20 and (d) x = 0.50. Conditions: 0.5 g prereduced catalyst, 5 g DPCD, 50 g cyclohexane as solvent, P = 3.5 MPa and T = 423 K. Full lines are calculated via integration of Equations (3)–(6) with initial conditions (7) and (8) and parameter estimates reported in Table 1; Figure S2: Data input for the Excel® tool; Figure S3: Example output in the presented Excel® tool. Line and column numbers (absent here) are actively noted in the tool itself. Table S1: Type of original data per literature source and equations to obtain data to be used in this work; Table S2: Catalyst systems, reaction times (h), conversion, C (%), selectivity, S (%) from Table 5 in reference [34]. Reaction conditions: S/C (substrate/catalyst) = 200, 2.0 MPa H_2, 298 K; Table S3: Cinnamaldehyde (CAL) conversion on different catalytic systems [35]. Reaction conditions: 0.2 g catalyst in 40 g of isopropanol, 5 w% CAL, 3.0 MPa H_2, 80 °C (Section 2.4, on p. 13 in the original article); Table S4: Product yield for hydrocinnamic aldehyde (HCAL), cinnamyl alcohol (COL), hydrocinnamic alcohol (HCOL) and others (Q) on Pd_CNT [35]. Reaction conditions: see Table S3. Yield is calculated via Equation (S2) and conversion and product selectivity are from original paper; Table S5: Product yield for hydrocinnamic aldehyde (HCAL), cinnamyl alcohol (COL), hydrocinnamic alcohol (HCOL) and others (Q) on Pd_CNT (A) [35]. Reaction conditions: see Table S3. Yield is calculated via Equation (S2) and conversion and product selectivity are from original paper; Table S6: Product yield for hydrocinnamic aldehyde (HCAL), cinnamyl alcohol (COL), hydrocinnamic alcohol (HCOL) and others (Q) on Pd_PNIPAM (L) [35]. Reaction conditions: see Table S3. Yield is calculated via Equation (S2) and conversion and product selectivity are from original paper; Table S7: Product yield for hydrocinnamic aldehyde (HCAL), cinnamyl alcohol (COL), hydrocinnamic alcohol (HCOL) and others (Q) on Pd_PNIPAM (H) [35]. Reaction conditions: see Table S3. Yield is calculated via Equation (S2) and conversion and product selectivity are from original paper; Table S8: Product yield for hydrocinnamic aldehyde (HCAL), cinnamyl alcohol (COL), hydrocinnamic alcohol (HCOL) and others (Q) on Pd_PNIPAM (LH) [35]. Reaction conditions: see Table S3. Yield is calculated via Equation (S2) and conversion and product selectivity are from original paper; Table S9: Hydrogenation data for the reaction of dicyclopentadiene (DCPD) into 8,9-dihydrocyclopentadiene (8,9-DHDCPD), *endo*-tetrahydrodicyclopentadiene (THDCPD) and C5 fraction (D) on $NiMo_{0.05}/\gamma$-Al_2O_3 catalyst (conversion of DCPD, X, and yield, Y) [36]. Reaction conditions: catalyst:DCPD:cyclcohexane = 1:10:100, 3.5 MPa H_2, 150 °C (Section 2.4, on p. 61 in the original article); Table S10: Hydrogenation data for the reaction of dicyclopentadiene (DCPD) into 8,9-dihydrocyclopentadiene (8,9-DHDCPD), *endo*-tetrahydrodicyclopentadiene (THDCPD) and C5 fraction (D) on $NiMo_{0.10}/\gamma$-Al_2O_3 catalyst (conversion of DCPD, X, and yield, Y) [36]. Reaction conditions: see Table S9; Table S11: Hydrogenation data for the reaction of dicyclopentadiene (DCPD) into 8,9-dihydrocyclopentadiene (8,9-DHDCPD), *endo*-tetrahydrodicyclopentadiene (THDCPD) and C5 fraction (D) on $NiMo_{0.20}/\gamma$-Al_2O_3 catalyst (conversion of DCPD, X, and yield, Y) [36]. Reaction conditions: see Table S9; Table S12: Hydrogenation data for the reaction of dicyclopentadiene (DCPD) into 8,9-dihydrocyclopentadiene (8,9-DHDCPD), *endo*-tetrahydrodicyclopentadiene (THDCPD) and C5 fraction (D) on $NiMo_{0.50}/\gamma$-Al_2O_3 catalyst (conversion of DCPD, X, and yield, Y) [36]. Reaction conditions: see Table S9; Table S13: Quantitative surface analysis of $NiMo_x/\gamma$-Al_2O_3 catalyst (x = 0.05, 0.10, 0.20 and 0.50); from original article Table 2, p. 64 [36]; Table S14: Comparison of proposed tool with currently available Excel® tools for kinetic modeling. The value n denotes different possible inputs, such as concentrations, pressures.

Author Contributions: Conceptualization, P.M.H.; methodology, P.M.H.; software, P.M.H.; validation, P.M.H. and D.Y.M.; formal analysis, P.M.H.; investigation, P.M.H. and D.Y.M.; data curation, P.M.H. and D.Y.M.; writing—original draft preparation, P.M.H.; writing—review and editing, P.M.H. and D.Y.M.; visualization, P.M.H. and D.Y.M.; supervision, P.M.H.; project administration, P.M.H. All authors have read and agreed to the published version of the manuscript.

Funding: This research was funded by BOF (Bijzonder Onderzoeksfonds, Ghent University), BOF.BAF.2025.0114.01.

Data Availability Statement: No new data were created or analysed in this study. Data sharing is not applicable to this article. The Excel® tool presented in this study is available upon request from the corresponding author.

Acknowledgments: P.M.H. acknowledges the Research and Development Program of Ghent University Global Campus (GUGC), Republic of Korea.

Conflicts of Interest: The authors declare no conflicts of interest.

Abbreviations

The following abbreviations are used in this manuscript:

A	compound A
AA	allyl alcohol
C	citral
CE	continuity equation
CAL	cinnamaldehyde
CN	citronellal
CNT	carbon nanotube
COL	cinnamyl alcohol
D	lump of cyclo-C5 compounds
DCPD	dicyclopentadiene
8,9-DHDCPD	8,9-dihydrocyclopentadiene
DMA	N,N-dimethylacetamide
DMF	N,N-dimethylformamide
GRG	generalized reduced gradient
HCAL	hydrocinnamic aldehyde
HCOL	hydrocinnamic alcohol
NIPAM	N-isopropylacrylamide
ODR	orthogonal distance regression
P	product, polymerization
Q	product
RSSQ	residual sum of squares
THDCPD	endo-tetrahydrodicyclopentadiene
XPS	X-ray photoelectron spectroscopy

References

1. Froment, G.F.; Hosten, L.H. Catalytic Kinetics: Modelling. In *Catalysis: Science and Technology*; Anderson, J.R., Boudart, M., Eds.; Catalysis—Science and Technology; Springer: Berlin/Heidelberg, Germany, 1981; pp. 97–170.
2. Froment, G.F.; Bischoff, K.B. *Chemical Reactor Analysis*, 2nd ed.; Wiley: New York, NY, USA, 1990.
3. Bertero, N.M.; Trasarti, A.F.; Apesteguía, C.R.; Marchi, A.J. Solvent effect in the liquid-phase hydrogenation of acetophenone over Ni/SiO_2: A comprehensive study of the phenomenon. *Appl. Catal. A* **2011**, *394*, 228–238. [CrossRef]
4. Bertero, N.M.; Trasarti, A.F.; Apesteguía, C.R.; Marchi, A.J. Liquid-phase dehydration of 1-phenylethanol on solid acids: Influence of catalyst acidity and pore structure. *Appl. Catal. A* **2013**, *458*, 28–38. [CrossRef]
5. Bertero, N.M.; Trasarti, A.F.; Moraweck, B.; Borgna, A.; Marchi, A.J. Selective liquid-phase hydrogenation of citral over supported bimetallic Pt–Co catalysts. *Appl. Catal. A* **2009**, *358*, 32–41. [CrossRef]
6. Busygin, I.; Wärna, J.; Toukomiitty, E.; Murzin, D.Y.; Leino, R. Hydrogenation of 1-phenyl-1,2-propanedione over Pt catalysts modified by cinchona alkaloid O-ethers and the kinetic resolution of the 1-hydroxyketones generated. *J. Catal.* **2008**, *254*, 339–348. [CrossRef]
7. Venkatesan, K.; Jayarama Krishna, J.V.; Anjana, S.; Selvam, P.; Vinu, R. Hydrodeoxygenation kinetics of syringol, guaiacol and phenol over H-ZSM-5. *Catal. Comm.* **2021**, *148*, 106164. [CrossRef]
8. Steinbach, D.; Kruse, A.; Sauer, J.; Vetter, P. Sucrose is a promising feedstock for the synthesis of the platform chemical hydroxymethylfurfural. *Energies* **2018**, *11*, 645. [CrossRef]

9. Swift, T.D.; Nguyen, H.; Anderko, A.; Nikolakis, V.; Vlachos, D.G. Tandem Lewis/Brønsted homogeneous acid catalysis: Conversion of glucose to 5-hydoxymethylfurfural in an aqueous chromium(III) chloride and hydrochloric acid solution. *Green Chem.* **2015**, *17*, 4725. [CrossRef]
10. Kumar, K.; Pathak, S.; Upadhyayula, S. 2nd generation biomass derived glucose conversion to 5-hydroxymethylfurfural and levulinic acid catalyzed by ionic liquid and transition metal sulfate: Elucidation of kinetics and mechanism. *J. Clean. Prod.* **2020**, *256*, 120292. [CrossRef]
11. Chen, K.; Khodakov, A.; Yang, J.; Bell, A.T.; Iglesia, E. Isotopic tracer and kinetic studies of oxidative dehydrogenation pathways on vanadium oxide catalysts. *J. Catal.* **1999**, *186*, 325–333. [CrossRef]
12. Hutchings, G.J.; Higgins, R. Effect of promoters on the selective oxidation of n-butane with vanadium-phosphorus oxide catalysts. *J. Catal.* **1996**, *162*, 153–168. [CrossRef]
13. Tanimu, G.; Abussaud, B.A.; Asaoka, S.; Alasiri, H. Kinetic study on n-butane oxidative dehydrogenation over the (Ni, Fe, Co)-Bi-O/γ-Al_2O_3 catalyst. *Ind. Eng. Chem. Res.* **2020**, *59*, 2773–2780. [CrossRef]
14. Kaluža, L.; Zdražil, M. Relative activity of Niobia-supported CoMo hydrodesulphurization catalyst prepared with NTA: A kinetic approach. *Catal. Comm.* **2018**, *107*, 62–67. [CrossRef]
15. Cantrell, D.G.; Gillie, L.J.; Lee, A.F.; Wilson, K. Structure-reactivity correlations in MgAl hydrotalcite catalysts for biodiesel synthesis. *Appl. Catal. A* **2005**, *287*, 183–190. [CrossRef]
16. Guliants, V.V. Structure-reactivity relationships in oxidation of C-4 hydrocarbons on supported vanadia catalysts. *Catal. Today* **1999**, *51*, 255–268. [CrossRef]
17. Wachs, I.E. Catalysis science of supported vanadium oxide catalysts. *Dalton Trans.* **2013**, *42*, 11762–11769. [CrossRef] [PubMed]
18. Rodriguez, J.A.; Stacchiola, D. Catalysis and the nature of mixed-metal oxides at the nanometer level: Special properties of MO_x/TiO_2(110) (M = V, W, Ce) surfaces. *Phys. Chem. Chem. Phys.* **2010**, *12*, 9557–9565. [CrossRef] [PubMed]
19. Bordes, E. The role of structural chemistry of selective catalysts in heterogeneous mild oxidation of hydrocarbons. *Comptes Rendus Acad. Sci. Ser. II C* **2000**, *3*, 725–733. [CrossRef]
20. Bordes, E. Synergistic effects in selective oxidation catalysis: Does phase cooperation result in site isolation? *Top. Catal.* **2001**, *15*, 131–137. [CrossRef]
21. Moriceau, P.; Taouk, B.; Bordes, E.; Courtine, P. Correlations between the optical basicity of catalysts and their selectivity in oxidation of alcohols, ammoxidation and combustion of hydrocarbons. *Catal. Today* **2000**, *61*, 197–201. [CrossRef]
22. Zee, D.Z.; Chantarojsiri, T.; Long, J.R.; Chang, C.J. Metal-polypyridyl catalysts for electro- and photochemical reduction of water to hydrogen. *Acc. Chem. Res.* **2015**, *48*, 2027–2036. [CrossRef] [PubMed]
23. Chirik, P.J. Iron- and cobalt-catalyzed alkene hydrogenation: Catalysis with both redox-active and strong field ligands. *Acc. Chem. Res.* **2015**, *48*, 1687–1695. [CrossRef] [PubMed]
24. Kulkarni, A.; Lobo-Lapidus, R.J.; Gates, B.C. Metal clusters on supports: Synthesis, structure, reactivity, and catalytic properties. *Chem. Comm.* **2010**, *46*, 5997–6015. [CrossRef] [PubMed]
25. Rendon, N.; Berthoud, R.; Blanc, F.; Gajan, D.; Maishal, T.; Basset, J.M.; Coperet, C.; Lesage, A.; Emsley, L.; Marinescu, S.C.; et al. Well-defined silica-supported Mo-alkylidene catalyst precursors containing one OR substituent: Methods of preparation and structure-reactivity relationship in alkene metathesis. *Chem. Eur. J.* **2009**, *15*, 5083–5089. [CrossRef] [PubMed]
26. Lee, E.L.; Wachs, I.E. In situ spectroscopic investigation of the molecular and electronic structures of SiO_2 supported surface metal oxides. *J. Phys. Chem.* **2007**, *111*, 14410–14425. [CrossRef]
27. Baron, M.; Abbott, H.; Bondarchuk, O.; Stacchiola, D.; Uhl, A.; Shaikhutdinov, S.; Freund, H.J.; Popa, C.; Ganduglia-Pirovano, M.V.; Sauer, J. Resolving the atomic structure of vanadia monolayer catalysts: Monomers, trimers, and oligomers on ceria. *Angew. Chem. Int. Ed.* **2009**, *48*, 8006–8009. [CrossRef] [PubMed]
28. Park, J.B.; Graciani, J.; Evans, J.; Stacchiola, D.; Ma, S.G.; Liu, P.; Nambu, A.; Sanz, J.F.; Hrbek, J.; Rodriguez, J.A. High catalytic activity of $Au/CeO_x/TiO_2$(110) controlled by the nature of the mixed-metal oxide at the nanometer level. *Proc. Natl. Acad. Sci. USA* **2009**, *106*, 4975–4980. [CrossRef] [PubMed]
29. Wang, J.B.; Tsai, D.H.; Huang, T.J. Synergistic catalysis of carbon monoxide oxidation over copper oxide supported on samaria-doped ceria. *J. Catal.* **2002**, *208*, 370–380. [CrossRef]
30. Liu, W.; Flytzani-Stephanopoulos, M. Total oxidation of carbon monoxide and methane over transition metal-fluorite oxide composite catalysts. 2. Catalyst characterization and reaction kinetics. *J. Catal.* **1995**, *153*, 317–332. [CrossRef]
31. Heynderickx, P.M.; Thybaut, J.W.; Poelman, H.; Poelman, D.; Marin, G.B. The total oxidation of propane over supported Cu and Ce oxides: A comparison of single and binary metal oxides. *J. Catal.* **2010**, *272*, 109–120. [CrossRef]
32. Klicpera, T.; Zdražil, M. Preparation of high-activity MgO-supported Co-Mo and Ni-Mo sulfide hydrodesulfurization catalysts. *J. Catal.* **2002**, *206*, 314–320. [CrossRef]
33. Gao, J.; Mo, X.H.; Goodwin, J.G. La, V, and Fe promotion of Rh/SiO_2 for CO hydrogenation: Detailed analysis of kinetics and mechanism. *J. Catal.* **2009**, *268*, 142–149. [CrossRef]

34. Mertens, P.G.N.; Cuypers, F.; Vandezande, P.; Ye, X.; Verpoort, F.; Vankelecom, I.F.J.; De Vos, D.E. Ag^0 and Co^0 nanocolloids as recycable quasihomogeneous metal catalysts for the hydrogenation of α,β-unsaturated aldehydes to allylic alcohol fragrances. *Appl. Catal. A* **2007**, *325*, 130–139. [CrossRef]
35. Zhu, J.; Dou, M.; Lu, M.; Xiang, X.; Ding, X.; Liu, W.; Li, M. Thermo-responsive polymer grafted carbon nanotubes as the catalyst support for selective hydrogenation of cinnamaldehyde: Effects of surface chemistry on catalytic performance. *Appl. Catal. A* **2019**, *575*, 11–19. [CrossRef]
36. Fang, Z.; Shi, D.; Li, A.; Wu, Q.; Wang, Q.; Zhao, Y.; Feng, C.; Jiao, Q.; Li, H. Probing the synergistic effect of Mo on Ni-based catalyst in the hydrogenation of dicyclopentadiene. *Appl. Catal. A* **2019**, *574*, 60–70. [CrossRef]
37. Trasarti, A.F.; Bertero, N.M.; Apesteguía, C.R.; Marchi, A.J. Liquid-phase hydrogenation of acetophenone over silica-supported Ni, Co and Cu catalysts: Influence of metal and solvent. *Appl. Catal. A* **2014**, *475*, 282–291. [CrossRef]
38. Gallezot, P.; Richard, D. Selective hydrogenation of α,β-unsaturated aldehydes. *Catal. Rev.-Sci. Eng.* **1998**, *40*, 81–126. [CrossRef]
39. Sun, Z.; Rong, Z.; Wang, Y.; Xia, Y.; Du, W.; Wang, Y. Selective hydrogenation of cinnamaldehyde over Pt nanoparticles deposited on reduced graphene oxide. *Appl. Catal. A-Gen.* **2014**, *4*, 1874–1878. [CrossRef]
40. Wang, W.; Chen, J.G.; Song, L.P.; Liu, Z.T.; Liu, Z.W.; Lu, J.; Xiao, J.L.; Hao, Z.P. One-step, continuous-flow, highly catalytic hydrogenation—isomerization of dicyclopentadiene to exo-tetrahydrodicyclopentadiene over Ni-supported catalysts for the production of high-energy-density fuel. *Energy Fuels* **2013**, *27*, 6339–6347. [CrossRef]
41. Sibi, M.G.; Singh, B.; Kumar, R.; Pendem, C.; Sinha, A.K. Single-step catalytic liquid-phase hydroconversion of DCPD into high energy density fuel exo-THDCPD. *Green Chem.* **2012**, *14*, 976–983. [CrossRef]
42. Hönicke, D.; Födisch, R.; Claus, P.; Olson, M. Cyclopentadiene and Cyclopentene. In *Ullmann's Encyclopedia of Industrial Chemistry*; Wiley-VCH Verlag GmbH & Co. KGaA: Weinheim, Germany, 2000. [CrossRef]
43. de Levie, R. Estimating parameter precision in nonlinear least squares with Excel's solver. *J. Chem. Educ.* **1999**, *76*, 1594–1598. [CrossRef]
44. Heynderickx, P.M. Activity coefficients for liquid organic reactions: Towards a better understanding of true kinetics with the synthesis of jasmin aldehyde as showcase. *Int. J. Mol. Sci.* **2019**, *20*, 3819. [CrossRef] [PubMed]
45. Heynderickx, P.M. Closing the balance by the CLOBAL procedure: Towards more accurate concentration, conversion and selectivity values. *Chem. Eng. J.* **2019**, *361*, 805–811. [CrossRef]
46. Heynderickx, P.M.; Thybaut, J.W.; Poelman, H.; Poelman, D.; Marin, G.B. Kinetic modeling of the total oxidation of propane over anatase and vanadia sputter deposited catalysts. *Appl. Catal. B* **2009**, *90*, 295–306. [CrossRef]
47. Heynderickx, P.M.; Thybaut, J.W.; Poelman, H.; Poelman, D.; Marin, G.B. Kinetic modeling of the total oxidation of propane over $CuO\text{-}CeO_2/\gamma\text{-}Al_2O_3$. *Appl. Catal. B* **2010**, *95*, 26–38. [CrossRef]
48. Rajashekharam, M.V.; Nikalje, D.D.; Jaganathan, R.; Chaudhari, R.V. Hydrogenation of 2,4-dinitrotoluene using a Pd/Al_2O_3 catalyst in a slurry reactor: A molecular level approach to kinetic modeling and nonisothermal effects. *Ind. Eng. Chem. Res.* **1997**, *36*, 592–604. [CrossRef]
49. Chen, J.G.; Sun, Z.; Balakotaiah, V.; Bollini, P. A global kinetic model for the oxidative dehydrogenation of ethane over mixed metal oxide catalysts at supra-ambient pressures. *Appl. Catal. A-Gen.* **2022**, *445*, 136605. [CrossRef]
50. Yadav, V.K.; Chauhan, K.Y.; Das, T. Spectroscopic and kinetic study of cyclohexane oxidation reaction in vapor phase over the catalyst $20FeMnO_\delta$/(3CeAl). *Ind. Eng. Chem. Res.* **2023**, *62*, 20170–20188. [CrossRef]
51. Nielsen, L.P.C.; Stevenson, C.P.; Blackmond, D.G.; Jacobsen, E.N. Mechanistic investigation leads to a synthetic improvement in the hydrolytic kinetic Rresolution of terminal epoxides. *J. Am. Chem. Soc.* **2005**, *126*, 1360–1362. [CrossRef] [PubMed]
52. Manaenkov, O.; Kosivtsov, Y.; Sapunov, V.; Kislitsa, O.; Sulman, M.; Bykov, A.; Sidorov, A.; Matveeva, V. Kinetic modeling for the "one-pot" hydrogenolysis of cellulose to glycols over $Ru@Fe_3O_4$/polymer catalyst. *Reactions* **2022**, *3*, 1–11. [CrossRef]
53. Gatti, M.N.; Perez, F.M.; Santori, G.; Pompeo, F. Glycerol hydrogenolysis to bio-propanol: Catalytic activity and kinetic model for Ni/C modified with $Al(H_2PO_4)_3$. *Reactions* **2023**, *4*, 679–701. [CrossRef]
54. Al-Sultami, A.H.; Al-Shathr, A.; Al-Zaidi, B.Y. Toluene alkylation reactions over Y-type zeolite catalysts: An experimental and kinetic study. *Reactions* **2024**, *5*, 1042–1065. [CrossRef]
55. Navidi, N.; Thybaut, J.W.; Marin, G.B. Experimental investigation of ethylene hydroformylation to propanal on Rh and Co based catalysts. *Appl. Catal. A* **2014**, *469*, 357–366. [CrossRef]
56. Acharya, A.; Dubbu, S.; Kumar, S.; Kumari, N.; Kim, Y.; So, S.; Kwon, T.; Wang, Z.; Park, J.; Cho, Y.-K.; et al. Atomically conformal metal laminations on plasmonic nanocrystals for efficient catalysis. *J. Am. Chem. Soc.* **2021**, *143*, 10582–10589. [CrossRef] [PubMed]